Acceleration of global N_2O emissions seen from two decades of atmospheric inversion

R. L. Thompson[1]*, L. Lassaletta[2], P. K. Patra[3], C. Wilson[4,5], K. C. Wells[6], A. Gressent[7], E. N. Koffi[8], M. P. Chipperfield[4,5], W. Winiwarter[9,10], E. A. Davidson[11], H. Tian[12] and J. G. Canadell[13].

1. Norsk Institutt for Luftforskning (NILU), Kjeller, Norway
2. CEIGRAM-Agricultural Production, Universidad Politécnica de Madrid, Madrid, Spain
3. Research Institute for Global Change, JAMSTEC, Yokohama 236 0001, Japan
4. National Centre for Earth Observation, University of Leeds, Leeds, UK
5. School of Earth and Environment, University of Leeds, Leeds, UK
6. Department of Soil, Water, and Climate, University of Minnesota, MN, USA
7. Massachusetts Institute of Technology, Cambridge, MA, USA
8. European Commission Joint Research Centre, Ispra, Italy
9. IIASA, Laxenburg, Austria
10. University of Zielona Góra, Poland
11. University of Maryland Center for Environmental Science, MD, USA
12. International Center for Climate and Global Change Research, School of Forestry and Wildlife Sciences, Auburn University, AL, USA
13. Global Carbon Project, CSIRO Oceans and Atmosphere, Canberra, Australia

*Corresponding author

Abstract

Nitrous oxide (N_2O) is the third most important long-lived greenhouse gas and an important stratospheric ozone depleting substance. Agricultural practices and the use of N-fertilizers have greatly enhanced emissions of N_2O. Here we present estimates of N_2O emissions determined from three global atmospheric inversion frameworks during 1998-2016. We find that globally N_2O emissions increased substantially from 2009 and at a faster rate than estimated by the Intergovernmental Panel on Climate Change (IPCC) emission factor (EF) approach. The regions of East Asia and South America made the largest contributions to the global increase. From the inversion-based emissions, we estimate a global EF of 2.3 ± 0.6%, which is significantly larger than the IPCC Tier-1 default for combined direct and indirect emissions of 1.375%. The larger EF and accelerating emission increase found from the inversions suggest that N_2O emission may have a non-linear response at global and regional scales with high levels of N-input.

Main text

Atmospheric N_2O has risen steadily since the mid-20th century[1,2], from approximately 290 ppb in 1940 to 330 ppb in 2017[3,4] - a trend strongly linked to the increase in reactive nitrogen (Nr) in the environment[5,6]. Nr creation has increased enormously since the mid-20th century largely owing to the Haber-Bosch process (used primarily to produce N-fertilizer), but also to the cultivation of N-fixing crops and the combustion of fossil and bio-fuels[7]. Although increased Nr availability has enabled large increases in food production, it is also associated with a number of environmental problems. Among these is the rise in N_2O emissions: Nr is the substrate of the microbial processes of nitrification and denitrification, both of which produce N_2O as a by-product[8].

N_2O emissions increased from 10-12 TgN y^{-1} prior to the industrial era[5,9] to an average of ~17 TgN/y in the last decade. Agriculture is responsible for the largest part of this change, with emissions increasing from 0.3-1.0 TgN y^{-1} in 1850 to 3.9-5.3 TgN y^{-1} in 2010[5,9,10]. In

order to meet ambitious climate targets, non-CO_2 greenhouse gas emissions will also require reductions[11]. For N_2O, this means reducing agricultural emissions while meeting the growing demand for food and other agricultural products. This will require changes in human diet and agricultural practices, and ultimately, improved nitrogen use efficiency (NUE), that is, increasing Nr in harvest relative to N-input[12,13].

N-input, in particular N-fertilizer use, is one of the best single predictors of N_2O emissions from agriculture with an estimated emission factor (EF) of ~1% based on emissions measured from soils[14]. Emission inventories, used for example in reporting under the United Framework Convention on Climate Change (UNFCCC), are based predominantly on the EF approach. For direct emissions from agricultural land, the default (Tier-1) value used in reporting to the UNFCCC is 1% with an uncertainty range from 0.3% to 3% owing to the variability with agricultural practices, soil properties, and meteorological conditions[14]. Similarly, EFs are used to estimate indirect N_2O emissions from ecosystems downstream and downwind of agricultural land, which receive Nr via run-off and atmospheric deposition, amounting to an additional but even more uncertain EF of ~0.375% (Ref 12).

Estimates of the global mean EF have also been made by relating observed changes in atmospheric N_2O to N-input, the so-called top-down approach, which includes emissions from agricultural land as well as downstream and downwind ecosystems. Top-down EF estimates vary from ~2 to 5% and strongly depend on the explanatory variable used, specifically whether it includes only newly fixed Nr or all Nr sources[5,15,16]. While there are differences between the modelled N_2O emissions depending on the explanatory variable, all EF approaches assume a linear response of N_2O to N-input. Conversely, evidence from field experiments suggests the emission response is often nonlinear where N-input is high[17-22]. However, whether a non-linear response of N_2O emissions is relevant at large scales and globally is unknown.

N_2O emissions can be estimated regionally independently of EFs using the atmospheric inversion approach, which utilizes spatiotemporal variations in atmospheric N_2O[23-25]. Here, we use a global network of N_2O observations to estimate N_2O emissions and their trends during 1998-2016. These are estimated using three independent inversion frameworks and transport models (see Supplementary Tables 1&2), providing a range of estimates representing the systematic uncertainty from errors in modelled transport and stratospheric N_2O loss (see Methods). Using updated datasets of N-input for the whole agricultural system (i.e. including crops and grasslands) and of N-surplus for cropping systems (i.e. the difference between N-input and Nr removed through harvest), we determine the response of the inversion-based emissions to these two explanatory variables and examine the linear assumption.

Emission trends and relation to N-input

From three inversions, we estimate a global mean emission of 17.0 (16.6-17.4) TgN y^{-1} for 1998 to 2016, with 11.3 (10.2-13.2) TgN y^{-1} from land and 5.7 (3.4-7.2) TgN y^{-1} from ocean (values in parentheses give the range over three inversions, Supplementary Table 3). The global emissions presented here are consistent with other top-down estimates ranging between 15.7 and 18.3 TgN y^{-1} for the year 2000[5,9,23-25]. Similarly, our land emissions estimate is within the range of other top-down estimates of 11.0 to 12.6 TgN y^{-1}, also for the year 2000[9,23-25], and the recent estimate from the Nitrogen Model Inter-comparison Project (NMIP)[10] of 10.0 ± 2.0 TgN y^{-1}.

Top-down methods, including atmospheric inversions, estimate the source as the sum of the observed change in atmospheric N_2O abundance and the amount lost in the stratosphere. As the stratospheric loss is not constrained directly by observations this term has considerable

uncertainty, which is propagated into the source estimate. We calculate that stratospheric loss contributes 1.1 TgN y^{-1} to the discrepancy in the source estimate based on the range of modelled atmospheric lifetimes, 118 to 129 years, and a median abundance of 1522 TgN (Supplementary Table 3) (the lifetimes and abundance are comparable to previous findings[26]). The discrepancy, however, is larger than the range in source estimates, indicating compensating effects in the inversions.

From 2000 the atmospheric growth rate increased steadily from a mean of 0.68 ppb y^{-1} for 2000-2005 to 0.98 ppb y^{-1} for 2010-2015, with significant bi- to tri-annual periodicity (Figure 1). Prior to 2000, calibration accuracy and measurement precision were significantly poorer, hence the growth rate for 1998 to 2000 is more uncertain. Our discussion, therefore, focuses on trends from 2000 onwards. Previous studies found a correlation between inter-annual variability in the growth rate and El Niño-Southern Oscillation (ENSO) and attributed it to changes in soil and ocean emissions[27,28]. El Niño is associated with lower growth rates, likely owing to reduced rainfall in tropical and subtropical regions[29] and suppressed upwelling in the eastern tropical Pacific[30]. One study also hypothesized an influence from stratosphere to troposphere transport on inter-annual variability[31]. The increasing trend, however, is likely due to increasing emissions; based on the inversions, emissions increased from 16.3 (15.5-17.1) TgN y^{-1} for 2000-2005 to 17.9 (17.3-18.5) TgN y^{-1} for 2010-2015. This increase is significantly larger than prior estimates, which showed an increase of 0.5 (0.4-0.6) TgN y^{-1}. A change of this magnitude cannot be explained by any known mechanism through the sink, as it would require an increase in atmospheric lifetime of ~20 years, and such a change is unrealistic over this time scale. The atmospheric models used in this study show no trend in lifetime for this period. The growth in emissions is 90% due to emissions over land (Figure 2) including the land-ocean aquatic continuum and inland water bodies (the spatial resolution of the inversions does not allow these components to be resolved separately).

An increase in emissions is consistent with global trends in total N-input and crop N-surplus, which grew by 59 and 18 TgN, respectively, during 2000-2013 (the last year for which data are available) (Figure 3). We include synthetic fertilizer applied to crop and grasslands and total animal excretion, biologically fixed nitrogen in crops and grassland, and NOx deposition from non-agricultural sources (Methods). A similar trend in N-input and N-surplus is seen for China, with increases of 15 and 8 TgN, respectively, as well as for South Asia (i.e., India, Nepal, Bangladesh and Pakistan) and to a lesser extent Brazil. We limit our focus to the global scale and the five countries/regions in Figure 2 because the inversions in other regions are not well constrained due to sparse observations and thus rely on the prior estimates.

The regional trends in N-input and N-surplus are consistent with the N_2O emissions derived from the inversions. Emissions were found to increase in China by 0.40 (0.34-0.47) TgN y^{-1} between 2000-2005 and 2010-2015 - significantly larger than prior estimates of 0.23 (0.18-0.32) TgN y^{-1}. Although there is an offset between INV1/INV2 and INV3 for Global land and China, the trends are very similar. The offset is largely due to residual dependence of the posterior on the prior estimates: INV3 used a larger land (and lower ocean) prior compared to INV1/INV2. The uncertainty in all regions was reduced by the inversions (Supplementary Figure 5). The change in South Asia was significantly smaller than in China, 0.14 (0.11-0.16) TgN y^{-1} but larger than indicated by prior estimates of only 0.03-0.05 TgN y^{-1}. In USA and Europe, emissions were fairly stable over the past nearly two decades. In Brazil, there was an increase between the two periods of 0.26 (0.23-0.29) TgN y^{-1}, but it was small compared to the year-to-year variability in emissions of 0.22 TgN y^{-1}. The five regions of focus account for ~50% of the global increase between the two time periods, while Africa accounts for ~20%, Central and South America (excluding Brazil) account for ~10%, Southeast Asia and

Oceania account for 8%, and 10% was due to changes in ocean emissions (Supplementary Figure 6).

Estimation of emission factors

Using the inversion emission trends and N-input data, we estimated EFs globally and regionally. To calculate EFs, we subtracted estimates of the non-soil emissions (i.e., from industry, energy and waste sectors from EDGAR-v4.3.2 (Supplementary Figure 7) and biomass burning from GFED-v4.1s) from the total emissions to give the contribution from soil, which we assume is proportional to N-input. Second, we subtracted the mean of the soil emissions from each inversion over 1998-2016 to remove any offset between inversions. Figure 4 shows scatter plots of N_2O emission anomalies from all inversions versus N-input. The linear regression coefficients provide an estimate of the EF for additional emissions resulting from additional N availability. The EFs were statistically significant ($P < 0.05$) globally, for China, Brazil and South Asia, but not for USA and Europe where changes in N-input and N_2O emission were small compared to the scatter in the data (Supplementary Table 4). The emissions are generally higher than proportionate (and more scattered) at the upper range of N-input globally and for China and Brazil, but using non-linear regressions led to only marginal improvements with no difference between quadratic versus exponential functions. Regressions were also calculated relative to N-surplus but no improvement in the correlation or reduction in the residual standard error was found (Supplementary Table 5 and Figure 8).

Globally, we find an EF of 2.3 ± 0.6% for the change in total soil N_2O emission relative to the change in total N-input, including N-fertilizer, manure, biological nitrogen fixation (BNF), and NOx deposition from non-agricultural sources (Figure 5). Our N-input differs slightly from the IPCC 2006 reporting guidelines, which includes (in addition to synthetic fertilizer and manure) Nr from crop residues and mineralization of soil organic matter where soil Nr stocks are changing due to land use or management[14]. On the other hand, our N-input includes total livestock excretion and not only that applied as manure as in the IPCC 2006 method. While the IPCC 2006 method does not directly include BNF, it assumes that Nr from BNF is relevant for N_2O production when left on fields in crop residue. We do not have estimates of Nr from mineralization of soil organic matter from land use or management, but this term is likely to be small compared to other N-inputs. Furthermore, our EF estimates assume that trends in natural emissions of N_2O are negligible over the study time period. Since changes in N_2O emissions due to anthropogenic N-input to natural ecosystems is counted as an anthropogenic emission, changes in natural N_2O emissions are primarily related to climatic changes. Natural emissions changed by an estimated 0.7 ± 0.5 TgN y^{-1} since the pre-industrial era and, therefore, likely have negligible impact on our EFs for 2000-2013[10].

The IPCC (Tier-1) method gives one EF for direct and another for indirect emissions, whereas we calculate the total EF relative to N-input. To compare the two methods, we estimate the IPCC total EF by adding the equations for direct and indirect emissions (using default parameters) and dividing by total N-input, giving an EF of 1.375% (see Methods). Our global mean EF is higher than the IPCC value but is sensitive to positive emission anomalies in 2010 and 2013 (Figure 2); excluding these values gives an EF that is not statistically different from the IPCC value. A longer time series of inversion-based emissions would help in determining the EF more accurately. However, our estimate of 2.3% agrees well with that of a previous top-down study[5], which found an EF of ~2.5% (Figure 5). Ref 5 estimated separate EFs for manure and N-fertilizer, of 2% and 2.5%, respectively, and found this gave a better fit to top-down estimated N_2O emissions throughout the 20th century compared to one EF for total N-input. This was because in the first half of the 20th century

Nr in manure was not only derived from contemporaneous N-fixation but was also mined from agricultural soils. Over the past two decades, N-mining from soils occurred only in a few countries, and manure Nr is predominantly derived from fertilizer Nr used to grow crops for livestock feed. Consistent with this, we find for the last nearly two decades that the fit to N_2O emissions did not improve if N-fertilizer and manure were considered separately as explanatory variables. A higher EF than the IPCC default, is also plausible considering the evidence of a non-linear response of N_2O emission to high levels of N-input[10,17-22], which is discussed below.

For China, we find an EF of 2.1 ± 0.4%, and this estimate is insensitive to emission anomalies. A high EF for China is credible given the very high rates of fertilizer application, low crop NUE (defined as the output/input ratio for cropping systems, Supplementary Figure 9), and possibility of a non-linear response of N_2O emission[10,17-22,32,33]. However, our EF for China is associated with systematic uncertainty owing to uncertain trends in non-soil emissions, in particular from industry, which differ substantially between inventories. If the non-soil emission trend is underestimated the EF would be overestimated and vice-versa. For example, using the GAINS inventory estimate for non-soil emissions (instead of EDGAR-v4.32), the EF for China would be only 1.4 ± 0.4% and not statistically different from the IPCC default. The most important difference between EDGAR and GAINS is the change in emissions from adipic acid production - in EDGAR these are reduced by ~90% between 2005 and 2010 whereas in GAINS they increase by a factor of ~2 (Supplementary Figure 7). The discrepancy arises from assumptions made about adipic acid plants that became operational after 2005, specifically their contribution to the total adipic acid production and what emission abatement technologies they use[34,35]. If the GAINS emissions were correct then the increase in emissions from adipic acid production would account for nearly 20% of the total increase in China's emissions since 2005. Trend differences between EDGAR and GAINS have negligible impact on the global EF calculation and for the other regions in our study.

For Brazil, we calculate an EF of 2.6 ± 0.7%. This value is sensitive to emission anomalies, specifically in 2010 and 2013 (as for the global EF). Removing these anomalies reduces the EF to 2.1 ± 0.7%. Our high EF for Brazil is puzzling due to the relatively high NUE, ~50%, a low portion of synthetic fertilizer in the total N-input, and predominantly low EF values measured at the plot scale (median 0.38%, range 0.13 to 5.14% in cropland)[36]. Several speculative explanations are possible, including insufficient field sampling of soil EFs among the rapidly changing agricultural management systems[37], declining NUE in expanding cereal production[38], underestimated BNF in pastures and sugar cane production[39], confounding effects of ENSO on the large emissions from Amazon forest soils or from fire[40], varying deforestation trends, as well as growth and intensification of cropland and livestock management[41,42].

For South Asia, we find an EF of 0.8 ± 0.4%, which was not sensitive to emission anomalies and is lower than the IPCC default. Although South Asia has a low NUE, it uses a much smaller portion of synthetic fertilizer in total N-input than China, and has lower intensity of synthetic fertilizer application over crop area, 96 kgN ha^{-1} compared to 281 kgN ha^{-1} in China for the mean over 2000-2013.

Evaluation of the emission factor approach

Globally, the inversion-based soil N_2O emissions grew at a faster rate than predicted with the IPCC Tier-1 EF from 2009 (Figure 6). The increase in emissions from 2000-2005 to 2010-2013, of 1.55 (1.44-1.71) TgN y^{-1}, is also more than double that predicted by the IPCC EF, of 0.59 TgN y^{-1}. Using the EF calculated here (2.3%) tended to overestimate the response between 2005-2009 and underestimate it after 2009, when the N-surplus was particularly

high. Although a non-linear (quadratic or exponential) function did not markedly improve the residual standard error in the regressions of N_2O emission versus N-input (owing to large scatter in the data), there are reasons to think the response may be non-linear, as suggested from field-based studies[17-22]. Mechanisms proposed for a non-linear response with large N-surplus include: 1) more available Nr substrate for nitrification and denitrification[43], 2) high soil concentrations of NO_3^- associated with a higher N_2O to N_2 ratio from denitrification[44], 3) Nr availability to microorganisms exceeding carbon availability leading to higher rates of N_2O emission[45], and 4) Nr stimulating microbial mobilization of N bound in soil organic matter[46]. We compared the inversion-based soil emissions with the non-linear models in Refs 17 and 18 (Supplementary Figure 10) and found that both give slightly higher estimates after 2009 compared to the IPCC EF, but still underestimate the emissions.

In China, the emissions similarly increased at a faster rate than estimated by the IPCC EF after 2009. Although the agreement is better in the scenario where the industrial emissions followed the trend in GAINS, if N-input remained at the same high level after 2013, then the IPCC Tier-1 EF would considerably underestimate the emissions also in this scenario from 2013. For Brazil, the IPCC EF again underestimates the growth in emissions after 2009, but for South Asia, it reproduces the trend seen in the inversion-based estimates.

USA and Europe differ from the other regions in that they have stable and decreasing N-input, respectively. In USA, the nearly flat inversion-based emissions are consistent with EF estimates. The notable negative emission anomaly for 2000-2005, however, is not captured, as it is not due to a change in N-input but rather likely to EF changes driven by meteorological conditions. Precipitation data[47] and the Palmer Drought Severity Index[48] (PDSI) for the USA in regions with non-negligible N_2O emissions show persistent dry conditions during 1999-2003, which may have led to a decrease in the EF during that time (Supplementary Figure 11). In the other regions studied, however, there was no clear relationship between N_2O emission anomaly and precipitation, PSDI, or soil temperature. For Europe, the emissions estimated using the EF approach are close to those from the inversions. Although the EF approach shows a small decrease, of 0.01 TgN y^{-1} between 2000-2005 and 2010-2013, no trend is seen in the inversion-based estimate, but it may be that any trend related to N-input is still too small to be captured by global scale inversions.

Conclusions and implications

N_2O emissions increased globally by 1.6 (1.4-1.7) TgN y^{-1} between 2000-2005 and 2010-2015, however the rate of increase from 2009 is underestimated using the IPCC Tier-1 default EF. We hypothesize that this is due to an increase in the EF associated with a growing N-surplus. This suggests that the Tier-1 method, which assumes a constant EF, may underestimate emissions when the rate of N-input and the N-surplus are high. This has been demonstrated at field scale, but here we show this likely also applies at regional and global scales. We therefore recommend moving towards IPCC Tier-2 approaches and using region-specific EFs, especially for high N-input and/or N-surplus conditions, but this would require a body of field measurements to determine accurate values for these EFs. Alternatively, process-based modelling (as used in the IPCC Tier-3 method) validated against observations could help estimate emissions where the N-input and/or N-surplus is high. Our results show that reducing N-surplus (and improving NUE) in high N-input regions should have a more than proportionate outcome in reducing N_2O emissions.

References (main text)

1. Ciais, P. *et al*. Carbon and Other Biogeochemical Cycles. In: *Climate Change 2013: The Physical Science Basis. Contribution of Working Group I to the Fifth Assessment Report of the Intergovernmental Panel on Climate Change* (2013).

2. Ravishankara, A. R., Daniel, J. S. & Portmann, R. W. Nitrous Oxide (N_2O): The Dominant Ozone-Depleting Substance Emitted in the 21st Century. *Science* **326**, 123–125 (2009).
3. Park, S. *et al*. Trends and seasonal cycles in the isotopic composition of nitrous oxide since 1940. *Nature Geosci* **5**, 261–265 (2012).
4. World Meteorological Organisation, *WMO Greenhouse Gas Bulletin* **14**, https://library.wmo.int/doc_num.php?explnum_id=5455 (2018).
5. Davidson, E. A. The contribution of manure and fertilizer nitrogen to atmospheric nitrous oxide since 1860. *Nature Geosci* **2**, 659–662 (2009).
6. Bouwman, A.F. *et al*. Global trends and uncertainties in terrestrial denitrification and N2O emissions. *Philos Trans R Soc B Biol Sci* **368**, 20130112 (2013).
7. Galloway, J. N. *et al*. The Nitrogen Cascade. *BioScience* **53**, 341-356 (2003).
8. Bremner, J. M. Sources of nitrous oxide in soils. *Nutrient Cycling in Agroecosystems* **49**, 7–16 (1997).
9. Syakila, A. & Kroeze, C. The global nitrous oxide budget revisited. *Greenhouse Gas Measurement and Management* **1**, 17–26 (2011).
10. Tian, H. *et al*. Global soil N_2O emissions since the pre-industrial era estimated by an ensemble of Terrestrial Biosphere Models: Magnitude, attribution and uncertainty. *Global Change Biology*, **25**, 640-659 (2018).
11. Masson-Delmotte, V. *et al*. Summary for Policymakers. In: Global warming of 1.5°C. An IPCC Special Report on the impacts of global warming of 1.5°C above pre-industrial levels and related global greenhouse gas emission pathways, in the context of strengthening the global response to the threat of climate change, sustainable development, and efforts to eradicate poverty, *World Meteorological Organization* (2018).
12. Davidson, E. A., Suddick, E. C., Rice, C. W. & Prokopy, L. S. More Food, Low Pollution (Mo Fo Lo Po): A Grand Challenge for the 21st Century. *Journal of Environment Quality* **44**, 305–7 (2015).
13. Springmann, M. *et al*. Options for keeping the food system within environmental limits. *Nature* **562**, 519-525 (2018).
14. De Klein, C. *et al*. in IPCC Guidelines for National Greenhouse Gas Inventories, Prepared by the National Greenhouse Gas Inventories Programme 4, 1–54 (2006).
15. Crutzen, P. J., Mosier, A. R., Smith, K. A. & Winiwarter, W. N_2O release from agro-biofuel production negates global warming reduction by replacing fossil fuels. *Atmos Chem Phys* **8**, 389–395 (2008).
16. Smith, K. A., Mosier, A. R., Crutzen, P. J. & Winiwarter, W. The role of N_2O derived from crop-based biofuels, and from agriculture in general, in Earth's climate. *Philos Trans Royal Soc B Biol Sci* **367**, 1169–1174 (2012).
17. Shcherbak, I., Millar, N. & Robertson, G. P. Global meta-analysis of the nonlinear response of soil nitrous oxide (N_2O) emissions to fertilizer nitrogen. *Proc Natl Acad Sci USA* **111**, 9199–9204 (2014).
18. Hoben, J. P. *et al*. Nonlinear nitrous oxide (N_2O) response to nitrogen fertilizer in on-farm corn crops of the US Midwest. *Global Change Biology* **17**(2), 1140–1152, (2010).
19. Signor, D., Cerri, C. E. P., & Conant, R. N_2O emissions due to nitrogen fertilizer applications in two regions of sugarcane cultivation in Brazil. *Environ Res Lett*, **8**(1), 015013 (2013).
20. Song, X., Liu, M., Ju, X., Gao, B., Su, F., Chen, X., & Rees, R. M. Nitrous Oxide Emissions Increase Exponentially When Optimum Nitrogen Fertilizer Rates Are

Exceeded in the North China Plain. *Environmental Science & Technology*, **52**(21), 12504–12513 (2018).

21. Philibert, A., Loyce, C., & Makowski, D. Quantifying Uncertainties in N2O Emission Due to N Fertilizer Application in Cultivated Areas. *PLoS One*, **7**(11), e50950 (2012).
22. Gerber, J. S., Carlson, K. M., Makowski, D., Mueller, N. D., Garcia de Cortazar-Atauri, I., Havlik, P., *et al*. Spatially explicit estimates of N_2O emissions from croplands suggest climate mitigation opportunities from improved fertilizer management. *Glob. Change Biol*., **22**(10), 3383–3394 (2016).
23. Saikawa, E. *et al*. Global and regional emissions estimates for N_2O. *Atmos Chem Phys* 14, 4617–4641 (2014).
24. Hirsch, A. I. *et al*. Inverse modeling estimates of the global nitrous oxide surface flux from 1998–2001. *Global Biogeochem. Cycles*, **20**, GB1008, doi:10.1029/2004gb002443 (2006).
25. Huang, J. *et al*. Estimation of regional emissions of nitrous oxide from 1997 to 2005 using multinetwork measurements, a chemical transport model, and an inverse method. *J. Geophys. Res*., **113**, D17313, doi:10.1029/2007JD009381 (2008).
26. Prather, M. J. *et al*. Measuring and modeling the lifetime of Nitrous Oxide including its variability. *J. Geophys. Res. Atmos*. **120**, 5693-5705 (2015).
27. Thompson, R. L. *et al*. Interannual variability in tropospheric nitrous oxide. *Geophys. Res. Lett*. **40**, 4426–4431 (2013).
28. Ishijima, K., Nakazawa, T. & Aoki, S. Variations of atmospheric nitrous oxide concentration in the northern and western Pacific. *Tellus B* **61**, 408–415 (2009).
29. Werner, C., Butterbach-Bahl, K., Haas, E., Hickler, T., & Kiese, R. A global inventory of N_2O emissions from tropical rainforest soils using a detailed biogeochemical model. *Global Biogeochem. Cycles*, **21**, GB3010 (2007).
30. Nevison, C. D., Mahowald, N. M., Weiss, R. F., & Prinn, R. G. Interannual and seasonal variability in atmospheric N_2O. *Global Biogeochem. Cycles*, **21**, GB3017 (2007).
31. Nevison, C. D. *et al*. Exploring causes of interannual variability in the seasonal cycles of tropospheric nitrous oxide. *Atmos. Chem. Phys*. **11**, 3713–3730 (2011).
32. Lassaletta, L. *et al*. 50 year trends in nitrogen use efficiency of world cropping systems: the relationship between yield and nitrogen input to cropland. *Environ. Res. Lett.* **9**, 105011 (2014).
33. Zhang, X. *et al*. Managing nitrogen for sustainable development. *Nature* **528**, 51-59 (2015).
34. Winiwarter, W. *et al*. Technical opportunities to reduce global anthropogenic emissions of nitrous oxide. *Environ Res Lett*, **13**(1), 014011 (2018).
35. Schneider, L., Lazarus, M., & Kollmuss, A. Industrial N_2O Projects Under the CDM: Adipic Acid - A Case of Carbon Leakage? Stockholm Environment Institute Working Paper WP-US-1006 (2010).
36. Meurer, K. H. E. *et al*. Direct nitrous oxide (N_2O) fluxes from soils under different land use in Brazil - a critical review. *Environ Res Lett* **11**(2), 023001 (2016).
37. Jankowski, K., C. *et al*. Deep soils modify environmental consequences of increased nitrogen fertilizer use in intensifying Amazon agriculture. *Scientific Reports*, **8**:13478 (2018).
38. Pires, M. V., da Cuhna, D. A., de Matos Carlos, S., & Heil Costa, M. Nitrogen-Use Efficiency, Nitrous Oxide Emissions, and Cereal Production in Brazil: Current Trends and Forecasts. *PLoS One*, **10**(8), 1–20 (2015). http://doi.org/10.1371/journal.pone.0135234

39. Herridge, D. F., Peoples, M. B., & Boddey, R. M. Global inputs of biological nitrogen fixation in agricultural systems. *Plant and Soil*, **311**(1-2), 1–18 (2008).
40. Davidson, E. A. *et al*. The Amazon basin in transition. *Nature*, **481**(7381), 321–328 (2012).
41. Zalles, V., *et al*. Near doubling of Brazil's intensive row crop area since 2000. *Proc Natl Acad Sci*. **22**, doi:10.1073/pnas.1810301115 (2018).
42. Merry, F., & Soares-Filho, B. Will intensification of beef production deliver conservation outcomes in the Brazilian Amazon? *Elem Sci Anth*, **5**, 24 (2017).
43. Van Groenigen, J. W. *et al*. Towards an agronomic assessment of N_2O emissions: a case study for arable crops. *European Journal of Soil Science*, **61**(6), 903–913 (2010).
44. Firestone, M. K. Biological Denitrification. In: *Nitrogen in Agricultural Soils, Agronomy Monograph* **22**, 289–326 (1982).
45. Firestone, M. K., & Davidson, E. A. Microbiological basis of NO and N_2O production and consumption in soil. In: *Exchange of Trace Gases Between Terrestrial Ecosystems and the Atmosphere*, M. O. Andreae & D. S. Schimel (Eds.), 7–21 (1989).
46. Kim, D.-G., Hernandez-Ramirez, G., & Giltrap, D. Linear and nonlinear dependency of direct nitrous oxide emissions on fertilizer nitrogen input: A meta-analysis. *Agriculture Ecosystems & Environment*, **168**, 53–65 (2013).
47. Adler, R. F. *et al*. The Version-2 Global Precipitation Climatology Project (GPCP) Monthly Precipitation Analysis (1979–Present). *J. Hydrometeor*, **4**(6), 1147–1167 (2003)
48. Dai, A. Characteristics and trends in various forms of the Palmer Drought Severity Index during 1900–2008. *J. Geophys. Res*. **116**(D12) (2011).

Methods

Emissions were estimated using three independent atmospheric inversion frameworks (see Supplementary Table 1). The frameworks all used the Bayesian inversion method, which finds the optimal emissions, that is, those, which when coupled to a model of atmospheric transport, provide the best agreement to observed N_2O mixing ratios while remaining with the uncertainty limits of the prior estimates. In other words, the emissions that minimize the cost function:

$$J(\mathbf{x}) = \frac{1}{2}\left(\mathbf{x}-\mathbf{x_b}\right)^{\mathrm{T}}\mathbf{B}^{-1}\left(\mathbf{x}-\mathbf{x_b}\right) + \frac{1}{2}\left(\mathbf{y}-H(\mathbf{x})\right)^{\mathrm{T}}\mathbf{R}^{-1}\left(\mathbf{y}-H(\mathbf{x})\right) \qquad (1)$$

where $\mathbf{x}$ and $\mathbf{x_b}$ are, respectively, vectors of the optimal and prior emissions, $\mathbf{B}$ is the prior error covariance matrix, $\mathbf{y}$ is a vector of observed N_2O mixing ratios, $\mathbf{R}$ is the observation error covariance matrix, and $H(\mathbf{x})$ is the model of atmospheric transport (for details on the inversion method see Ref. 49). The optimal emissions, $\mathbf{x}$, were found by solving the first order derivative of equation (1):

$$J'(\mathbf{x}) = \mathbf{B}^{-1}\left(\mathbf{x}-\mathbf{x_b}\right) + \left(H'(\mathbf{x})\right)^{\mathrm{T}}\mathbf{R}^{-1}\left(\mathbf{y}-H(\mathbf{x})\right) = 0 \qquad (2)$$

where $(H'(\mathbf{x}))^{\mathrm{T}}$ is the adjoint model of transport. In frameworks INV1 and INV2, equation (2) was solved using the variational approach[50,51], which uses a descent algorithm and computations involving the forward and adjoint models[52]. In framework INV3, equation (2) was solved directly by computing a transport operator, $\mathbf{H}$ from integrations of the forward model, such that $\mathbf{Hx}$ is equivalent to $H(\mathbf{x})$, and taking the transpose of $\mathbf{H}$[53].

Each of the inversion frameworks used a different model of atmospheric transport with different horizontal and vertical resolutions (see Supplementary Table 1). The transport

models TOMCAT and LMDz, used in INV1 and INV2 respectively, were driven by ECMWF ERA-Interim wind fields, and the model, MIROC4-ACTM, used in INV3, was driven by JRA-55 wind fields. While INV1 and INV2 optimized the emissions at the spatial resolution of the transport model, INV3 optimized the error in the emissions aggregated into 84 land and ocean regions[53]. All frameworks optimized the emissions with monthly temporal resolution. The transport models included an online calculation of the loss of N_2O in the stratosphere due to photolysis and oxidation by $O(^1D)$ resulting in mean atmospheric lifetimes of between 118 and 129 years, broadly consistent with recent independent estimates of the lifetime of 116 ± 9 years[26].

The inversions used N_2O measurements of discrete air samples from the National Oceanic and Atmospheric Administration Carbon Cycle Cooperative Global Air Sampling Network (NOAA) and the Commonwealth Scientific and Industrial Research Organisation network (CSIRO). In addition, we used measurements from in-situ instruments in the Advanced Global Atmospheric Gases Experiment network (AGAGE), the NOAA CATS network, and from individual sites operated by University of Edinburgh (UE), National Institute for Environmental Studies (NIES) and the Finish Meteorological Institute (FMI) (see Supplementary Figure 1). Measurements from networks other than NOAA were corrected to the NOAA calibration scale, NOAA-2006A[54], using the results of the WMO Round Robin inter-comparison experiment (https://www.esrl.noaa.gov/gmd/ccgg/wmorr/). Frameworks INV1 and INV2 used a total of 83 discrete air sampling sites, 15 in-situ sampling sites and discrete air samples from the NOAA network of ships and moorings, and INV3 used 37 discrete air sampling sites. Daily average observations were assimilated in INV1 and INV3, while INV2 assimilated hourly afternoon values for low altitude sites and nighttime values for mountain sites to minimize errors in the modeled mixing ratios from errors in the modeled planetary boundary layer heights and local mountain-valley circulation.

Each framework applied its own method for calculating the uncertainty in the observation space, the square of which gives the diagonal elements of the observation error covariance matrix **R**. The observation space uncertainty accounts for measurement and model representation errors and is equal to the quadratic sum of these terms. INV1 assumed a measurement uncertainty of 0.4 ppb and, in addition, estimated the model representation error as the mixing ratio gradient across the grid cell in which the observation is located and the surrounding ones, resulting in a mean total uncertainty of 0.48 ppb. INV2 assumed a measurement uncertainty of 0.3 ppb and estimated the representation error in the same way as INV1, resulting in a mean total uncertainty of 0.50 ppb. INV3 used a measurement uncertainty of 0.32 ppb and estimated the representation error as 1-sigma standard deviation of daily observations at each site.

Prior emissions were used in all frameworks and were based on existing estimates from terrestrial biosphere and ocean biogeochemistry models as well as from inventories (see Supplementary Table 2). INV1 and INV2 used the same prior estimates for emissions from natural and agricultural soils from the model OCN-v1.1, for ocean emissions from the model PlankTOM5, and for biomass burning emissions from the Global Fire Emissions Database (GFED-v4.1s). OCN parameterizes N_2O emissions from nitrification and denitrification in soils and accounts for N-input from N-fertilizer, manure, atmospheric deposition, and biological nitrogen fixation. The model is driven by CRU-NCEP meteorological data and uses inter-annually varying N-input[55]. PlankTOM5 uses the observed correlation between apparent oxygen utilisation and excess N_2O in oxic waters to estimate the open ocean source of N_2O production and the increased yield of N_2O in suboxic waters from both nitrification and denitrification as an additional source in oxygen minimum zones[56]. The model, PlankTOM5, is incorporated into the ocean general circulation model, NEMO v3.1, which is

forced with NCEP meteorology. For non-soil anthropogenic emissions (namely those from energy, industry and waste sectors), both INV1 and INV2 use the Emission Database for Greenhouse Gas Research (EDGAR) but differing versions (see Supplementary Table 2). INV3 used GEIA (Global Emissions Initiative) for emissions from natural soils and ocean emissions from Manizza et al. 2012[57]. Manizza et al. model ocean emission using the correlation of apparent oxygen utilization and excess N_2O in oxic waters and their model is incorporated into the MIT General Circulation Model. For soil and non-soil anthropogenic emissions, INV3 used a third version of EDGAR (see Supplementary Table 2), which also includes agricultural burning but they did not specifically account for wildfire emissions in the prior estimates.

Prior uncertainties were estimated in all the inversion frameworks for each grid cell (INV1 and INV2) or for each region (INV3) and square of the uncertainties formed the diagonal elements of the prior error covariance matrix **B**. INV1 and INV2 estimated the uncertainty as proportional to the prior value in each grid cell, and INV2 set lower and upper limits for the uncertainty of 3×10^{-9} and 5×10^{-8} kgN m^{-2} h^{-1}, respectively. INV3, on the other hand, set the uncertainty uniformly for the land regions at 1 TgN y^{-1} and for the ocean regions at 0.5 TgN y^{-1}. INV2 was the only framework to account for spatial and temporal correlations in the errors (resulting in off-diagonal elements in the prior error covariance matrix) using an exponential decay model with distance and time with correlation scale lengths of 500 km over land and 1000 km over ocean and 90 days.

The optimized emissions were interpolated to 1°×1° (see Supplementary Figure 2) and the regional emissions were calculated by integrating the gridded emissions within each region or country. For each region, estimates of the non-soil anthropogenic emissions (i.e., from industry, energy and waste sectors) from EDGAR-v4.32 and the biomass burning emissions from GFED-v4.1s were subtracted from the total emissions from the inversions to give only the contribution from soil, which is assumed to be proportional to N-input. This assumes that the error in the estimate for non-soil anthropogenic emissions is substantially smaller than that in the soil emissions (Supplementary Figure 7).

The inversions were validated by integrating the forward models with the posterior emissions and comparing the simulated mixing ratios with independent observations, i.e., observations that were not assimilated in the inversions. We compared with CONTRAIL (Comprehensive Observation Network for TRace gases by AirLiner, http://www.jal-foundation.or.jp/shintaikikansokue/contrail_index.htm), which has N_2O observations at regular intervals across the Pacific since 2005 (Supplementary Figure 3). All three inversions showed a similar level of performance with differences typically of <0.5 ppb. We also compared with aircraft profile measurements over USA from NOAA from sites with data for the early 2000s (Supplementary Figure 4). We found that INV1 tended to underestimate N_2O in the lower troposphere over the contiguous USA for the early 2000s, hence we did not include the emissions data for USA prior to 2005 in our analyses.

We calculated N inputs to the whole agricultural system including crops and grasslands. Total inputs correspond to synthetic fertilizer application, animal excretion (even if finally not reaching crops or grasslands), biological nitrogen fixation, and NOx deposition on agricultural land. Total outputs correspond to crop and animal production. Total surplus is calculated as the difference between inputs and outputs. In this budget, we neglected the small part of crop production that is locally consumed by livestock. Synthetic fertilizer application is based on the FAOSTAT dataset (http://www.fao.org/home/en/) with several inputs from the International Fertilizer Association (https://www.fertilizer.org/). Total animal excretion is calculated using the FAOSTAT livestock inventory and dynamic excretion factors, biological N fixation is calculated from crop productivities[58] and

atmospheric deposition was from Ref 59. Grassland nitrogen fixation was based on the grassland production estimated following Ref 60 and validated through comparison with the IMAGE model[61]. We consider 20% of grass species to be N fixing legumes and that their N fixation is equal to 1.4 times the N from aerial production to also account for below ground biomass production, which would otherwise not be included[58]. N output in harvested crops is based on crop productivity and N content of 177 crops, utilizing data from the FAOSTAT database. See also the detailed methodology in Refs 32 and 60. We consider the N-surplus and NUE of cropping systems, as they are widely used as an indicator of the agronomic and environmental performance of agricultural systems.

Emission factors were determined by a linear regression of N_2O soil emission versus total N-input. The total N-input consisted of sources of N from synthetic fertilizer (N_{SF}), organic fertilizer and manure (N_{ON}), biological nitrogen fixation (N_{BNF}) and NOx deposition from non-agricultural sources. This emission factor represents the total of direct and indirect emissions. The emission factors calculated in this study were compared to the IPCC Tier-1 default values, where the total IPCC EF was calculated by taking the weighted average of the direct (EF_{dir}) and indirect factors for deposition (EF_{dep}) and leaching (EF_{leach}) according to:

$$EF_{tot} = EF_{dir} + EF_{dep}\left(f_{SF}\frac{N_{SF}}{N_{tot}} + f_{ON}\frac{N_{ON}}{N_{tot}} \right) + EF_{leach} f_{leach} \qquad (3)$$

where f_{SF} and f_{ON} are the fractions of synthetic and organic fertilizer volatized, respectively, and f_{leach} is the fraction of N lost by leaching and runoff [12]. The modelled N_2O emission (F_{N2O}) using the IPCC emission factors was calculated as:

$$\begin{aligned} F_{N_2O} = {} & EF_{dir}\left(N_{SF} + N_{ON} + N_{BNF}\right) + EF_{dep}\left(N_{SF} f_{SF} + N_{ON} f_{ON}\right) + \\ & EF_{leach}\left(N_{SF} + N_{ON} + N_{BNF}\right) f_{leach} \end{aligned} \qquad (4)$$

using the N-input dataset described above.

References (Methods)

49. Tarantola, A. *Inverse problem theory and methods for model parameter estimation*. Society for Industrial and Applied Mathematics (2005).
50. Thompson, R. L. *et al*. Nitrous oxide emissions 1999 to 2009 from a global atmospheric inversion. *Atmos. Chem. Phys*. **14**, 1801–1817 (2014).
51. Wilson, C., Chipperfield, M. P., Gloor, M., & Chevallier, F. Development of a variational flux inversion system (INVICAT v1.0) using the TOMCAT chemical transport model. *Geosci Model Dev* **7(**5), 2485–2500 (2014).
52. Fisher, M. & Courtier, P. Estimating the covariances matrices of analysis and forecast error in variational data assimilation. *Technical Memorandum of the European Centre for Medium-Range Weather Forecasts* **220**, 1-26 (1995).
53. Patra, P. K. *et al*. Improved Chemical Tracer Simulation by MIROC4.0-based Atmospheric Chemistry-Transport Model (MIROC4-ACTM). *SOLA* **14**, 91–96 (2018).
54. Hall, B. D., Sutton, G. S. & Elkins, J. W. The NOAA nitrous oxide standard scale for atmospheric observations. *J Geophys Res* **112**, D09305 (2007).
55. Zaehle, S., Ciais, P., Friend, A. D. & Prieur, V. Carbon benefits of anthropogenic reactive nitrogen offset by nitrous oxide emissions. *Nature Geosci* **4**, 601–605 (2011).
56. Suntharalingam, P. *et al*. Quantifying the impact of anthropogenic nitrogen deposition on oceanic nitrous oxide. *Geophys. Res. Lett*. **39**, L07605 (2012).

57. Manizza, M., Keeling, R. F. & Nevison, C. D. On the processes controlling the seasonal cycles of the air–sea fluxes of O_2 and N_2O: A modelling study. *Tellus B: Chemical and Physical Meteorology* **64**, 18429 (2012).
58. Anglade, J., Billen, G., & Garnier, J., Relationships for estimating N_2 fixation in legumes: incidence for N balance of legume-based cropping systems in Europe. *Ecosphere* **6**, 37 (2015).
59. Dentener, F. *et al*. Nitrogen and sulfur deposition on regional and global scales: A multimodel evaluation. *Global Biogeochem. Cycles*, **20**(4) (2006).
60. Lassaletta, L. *et al*. Nitrogen use in the global food system: Past trends and future trajectories of agronomic performance, pollution, trade, and dietary demand. *Environ. Res. Lett.* **11**. (2016).
61. Stehfest, E. *et al*. Integrated Assessment of Global Environmental Change with IMAGE 3.0. Model Description and Policy Applications. Netherlands Environmental Assessment Agency, The Hague (2014).
62. Le Noë, J., Billen, G., & Garnier, J. How the structure of agro-food systems shapes nitrogen, phosphorus, and carbon fluxes: The generalized representation of agro-food system applied at the regional scale in France. *Science of the Total Environment*, **586**, 42–55 (2017).

Acknowledgements

We kindly acknowledge the people and institutions who provided atmospheric observations of N_2O that were used in the inversions or for validation, namely: E. Dlugokencky, G. Dutton, C. Sweeney (NOAA); J. Mühle (UCSD), P. Krummel, P. Fraser, L. P. Steele, R. Wang (CSIRO); S. O'Doherty, D. Young (Bristol University); Y. Tohjima, T. Machida (NIES); T. Laurila, J. Hatakka, T. Aalto (FMI); J. Moncrieff (University of Edinburgh); and H. Matsueda, Y. Sawa (MRI-JMA). The atmospheric observations can be accessed from WDCGG (https://gaw.kishou.go.jp), NOAA (https://www.esrl.noaa.gov/gmd/) and AGAGE (https://agage.mit.edu) websites. Precipitation and PDSI data are provided by the NOAA/OAR/ESRL PSD, Boulder, Colorado, USA, from their website at https://www.esrl.noaa.gov/psd/. AGAGE is supported principally by NASA (USA) grants to MIT and SIO, and also by BEIS (UK) and NOAA (USA) grants to Bristol University, CSIRO and BoM (Australia); FOEN grants to Empa (Switzerland), NILU (Norway), SNU (Korea), CMA (China), NIES (Japan), and Urbino University (Italy). We thank W. Feng (NCAS Leeds) for TOMCAT model support. L. L. Lassaletta is supported by MINEC-Spain and European Commission ERDF Ramón y Cajal grant (RYC-2016-20269), Programa Propio from UPM, and acknowledges the Comunidad de Madrid (Spain) and structural funds 2014-2020 (ERDF and ESF), project AGRISOST-CM S2018/BAA-4330. R. Thompson acknowledges financial support from VERIFY (grant no. 76810) funded by the European Commission under the H2020 programme, H. Tian acknowledges support from OUC-AU Joint Center. P. Patra is partly supported by the Environment Research and Technology Development Fund (#2-1802) of the Ministry of the Environment, Japan. The authors are grateful to the reviewers and to Profs. G. Billen and J. Garnier for useful comments, and to the Food and Agriculture Organization of United Nations (FAO) for providing global statistics and data through FAO Statistics (FAOSTAT).

Author contributions

RLT designed the study, contributed inversion results and prepared the manuscript; LL prepared the N-data and contributed to the manuscript; PKP, CW and MPC contributed inversion results and to the manuscript; KCW, AG, ENK, WW and EAD helped with the analysis and contributed to the manuscript; HT and JCG contributed to the manuscript.

Competing interests statement

The authors declare that they have no competing interests.

Data availability

Atmospheric observations used in the inversions are available from the databases indicated in the Acknowledgements. The CONTRAIL data used in the validation of the inversion results are available on request to H. Matsueda (MRI-JMA). The inversion output data are available from http://doi.org/10.5281/zenodo.3384591 and the N-data are available from https://doi.org/10.5281/zenodo.3384678. The inversion codes are available from the following authors on reasonable request: C. Wilson (c.wilson@leeds.ac.uk) for INV1; R. Thompson (rlt@nilu.no) for INV2; and P. Patra (prabir@jamstec.go.jp) for INV3.

Figure 1. Observed and modelled global mean growth rates of N_2O. Observed growth rates are shown based on the NOAA discrete sampling network and, for comparison, the AGAGE network. Modelled growth rates were calculated by sampling 4D mixing ratio fields at the times and locations of the NOAA observations. All growth rates were calculated with annual time steps and are shown as 1-year running averages.

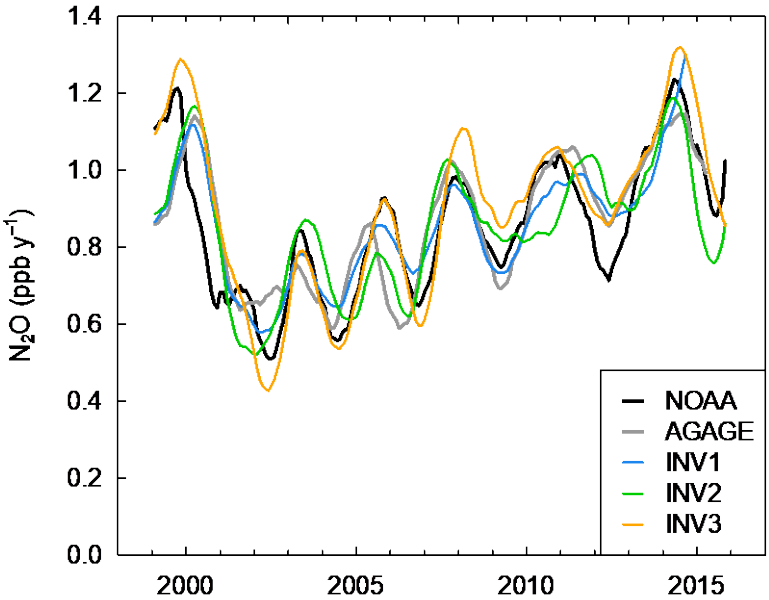

Figure 2. Annual N_2O emissions from the atmospheric inversions for 1998 to 2016 (units TgN y^{-1}). Dashed lines show the prior and solid lines the posterior emissions. INV1 data prior to 2005 for USA are shown as a dotted line as these data are more uncertain (see Methods).

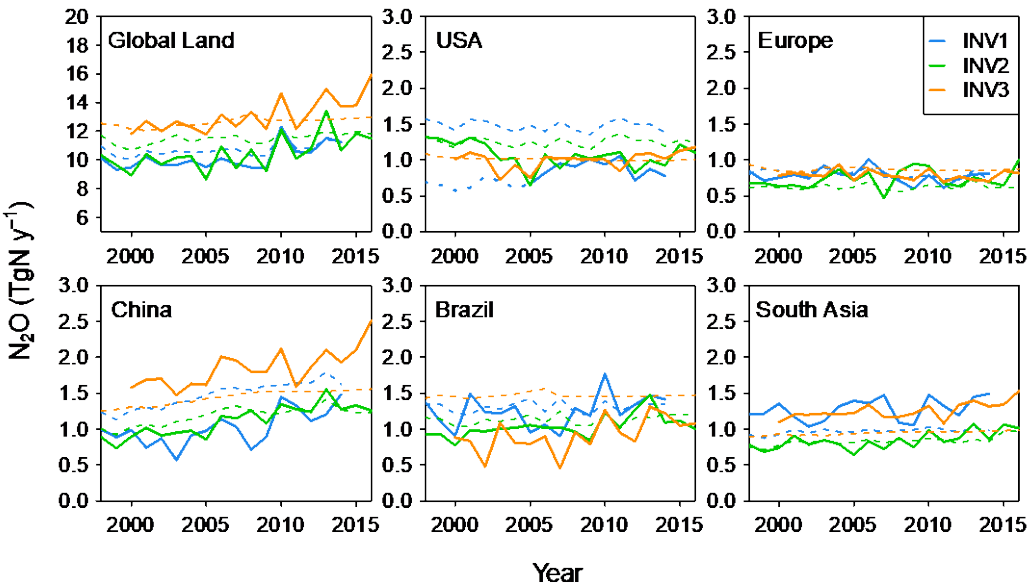

Figure 3. N-inputs to world crops and grasslands (units TgN y^{-1}) and N-surplus in the cropping systems. (N-fert is synthetic fertilizer, N-fixed is biologically fixed N, NOx-dep is NOx deposition, N-surplus is surplus only for cropping systems).

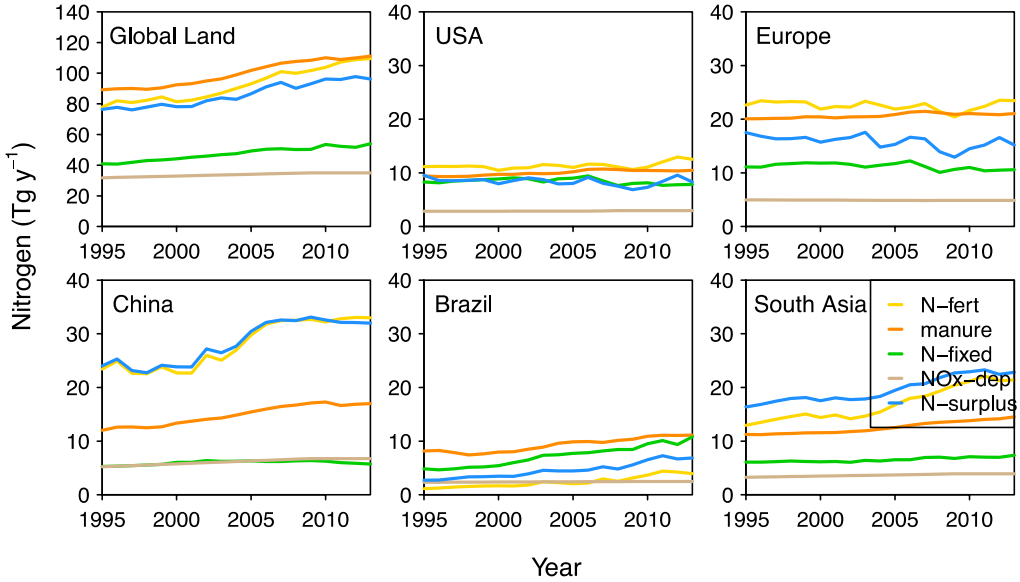

Figure 4. Scatter plots of the N_2O emission anomalies versus N-input (units TgN y^{-1}). The emissions were corrected for the non-soil component and the anomalies were calculated relative to the mean for 1998 to 2013. The symbols are colour-coded by year (circles = INV1, squares = INV2, diamonds = INV3). The solid line shows the regression and the dotted lines the confidence range. In the case that the regression is not significant ($P > 0.05$) a dashed line is used for the regression. (INV1 was excluded for USA owing to the poorer model-observation comparison for 1998-2005).

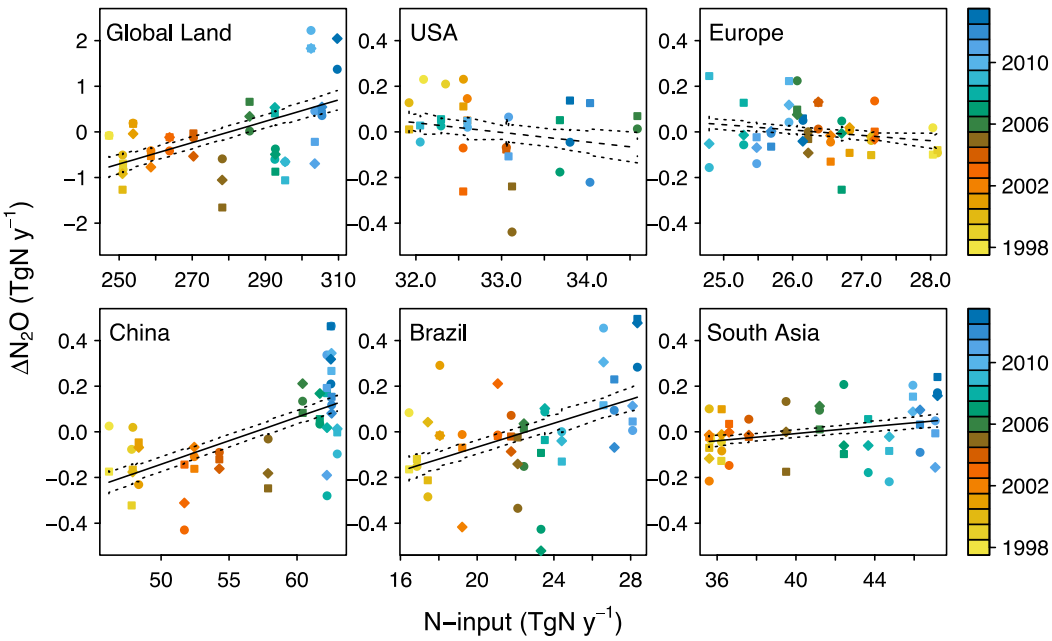

Figure 5. Comparison of emission factors (EF) from this study and from recent literature. The white to red circles are the EFs calculated over all inversions in this study and the colour indicates the correlation coefficient (see legend). The grey points are the EFs calculated from the individual inversions where the correlation was significant (circles = INV1, squares = INV2, diamonds = INV3). A second EF is shown (red diamond) for China using the GAINS estimate for the non-soil anthropogenic emissions. For the values reported by this study, the error bars show the standard error and for the other studies, they show the reported uncertainty.

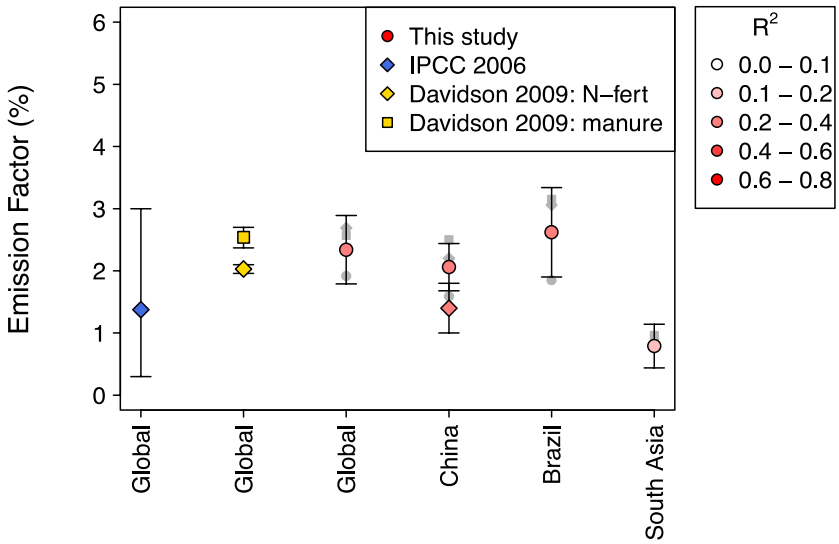

Figure 6. Comparison of N_2O emissions from the inversions (corrected for the non-soil component) with those calculated using the EF approach (units TgN y^{-1}). The inversion results are shown as the mean (black line) and range (grey shading). A scalar value was added to the emissions time series' so that they matched the inversion mean in the year 2000. The EF results are shown using the IPCC value (blue) and the linear fit from this study (green). For USA and Europe the regional EFs from this study were not significant so the global EF from this study was used instead. For China, the emissions corrected using GAINS for the non-soil component (instead of EDGAR-v4.32) are also shown (black dotted line).